01,08,13

Study of the baric and temperature dependences of the monocrystalline tantalum properties

© M.N. Magomedov

Institute for geothermal problems and renewable energy —
branch of the joint Institute of high temperatures of the Russian Academy of Sciences,
Makhachkala, Russia

E-mail: mahmag4@mail.ru

Received September 19, 2025
Revised September 19, 2025
Accepted October 2, 2025

The equation of state, as well as the baric and temperature dependences of the thermoelastic and surface properties of monocrystalline tantalum, were calculated using an analytical method (i.e., without computer simulation). This method is based on the paired interatomic four-parameter Mie–Lennard-Jones potential and takes into account the contributions of both the lattice and electronic subsystems of the metal. Using this method, the baric and temperature dependences of the isothermal elastic modulus, thermal expansion coefficient, isobaric heat capacity, and derivatives of these functions with respect to pressure were calculated. The baric dependences are calculated along the isotherms $T = 300$ and 3000 K, and the temperature dependences are calculated along the isobars $P = 0$ and 100 GPa. It is shown that the calculated dependencies are in good agreement with the dependencies obtained both experimentally and using computer simulating. For the first time, the surface properties of tantalum have been calculated: the specific surface energy, as well as its derivatives in temperature and pressure. The tantalum properties have been studied under $P-T$ conditions which hard-to-reach for the experiment, and it was found out in which $P-T$ arguments the electronic contribution to these properties is noticeable, and in which area its influence on the tantalum properties can be neglected.

Keywords: tantalum, equation of state, elastic modulus, thermal expansion, surface energy, electronic subsystem, Debye temperature, Grüneisen parameter.

DOI: 10.61011/PSS.2025.10.62621.260-25

1. Introduction

Tantalum (tantalum, Ta) got its name because of the difficulties in its fabrication and its further purification from impurities. In its pure form metallic tantalum was obtained only early inXX. At the atmospheric pressure the melting temperature of tantalum is equal $T_m(P = 1\,\text{bar}) = 3296 \pm 20\,\text{K}$ [1] which allows to refer it to the refractory metals. Its high corrosion resistance and ductility (almost like that of gold) have made it very popular for the fabrication of parts operating at high temperatures and aggressive environments. In some cases, tantalum may successfully replace more expensive platinum, thus finding application both in jewelry and in the manufacture of measuring standards. Tantalum is also an excellent getter (gas absorber): at 800 °C, it is able to absorb 740 volumes of gas. Ta becomes superconducting at temperatures below 4.45 K. Ta is also featuring high biological compatibility with living tissues, which explains the widespread use of Ta in medicine.

The unique properties of tantalum have been studied for a long time, both experimentally and theoretically [1–13]. At the same time, due to the difficulties of purifying tantalum from impurities, many of its properties have either been experimentally studied very little or not studied at all. For example, the literature has no data about a dependence of a specific surface energy σ of tantalum on neither the temperature T nor the pressure P. That being said, the increasing use of Ta in various fields of science and technology requires a comprehensive study of these properties of Ta under various $P-T$ conditions. Moreover, if the equation of state, elastic modulus, thermal expansion, and heat capacity of monocrystalline Ta have recently been studied in detail [7–13], then no one has studied the surface properties of Ta under various $P-T$-conditions. Meanwhile, it is the surface properties that determine the strength and adhesive properties of the crystal. In this regard, in this paper, using the analytical method (i.e. without computer modeling), which was presented in [14–16], the equation of state, elastic modulus, thermal expansion, heat capacity, and surface properties of Ta were calculated from a unified perspective. Moreover, in this paper, the method from [14–16] is generalized to account for the contribution of thermally excited electrons. This allowed us to study the question of which properties of tantalum are significantly affected by accounting for the electronic subsystem (ELS), and which properties are not affected by accounting for ELS. Here, for the first time, the pressure dependences of thermoelastic and surface properties of Ta were calculated along two isotherms, 300 and 3000 K, from 0 to 300 GPa, and the temperature dependences of these properties of Ta were calculated along two isobars: 0 and 100 GPa,

from 10 to 3300 K. This allowed to study the properties of tantalum in the hard-to-reach for experiment $P-T$-conditions, and also to identify, in which domain of $P-T$-arguments the ELS contribution is noticeable, and in which domain of $P-T$-parameters the ELS effect on Ta properties may be neglected.

2. Calculation method

Our analytical method of calculation of the single-component crystal properties was presented in detail in [14–16]. However, this method did not take into account the effect of ELS on the properties of metal. For dielectric materials and low-melting metals, the method from [14–16] has shown good results. However, for studying some thermodynamic properties of refractory metals, the contribution of ELS turns out to be significant, especially at low pressures and high temperatures. Therefore, in this study we've generalized the method from [14–16] to account the ELS contribution for metal.

In order to describe pairwise interatomic interaction, this method uses a four-parameter Mie–Lennard-Jones potential, which is expressed as follows:

$$\varphi(r) = \frac{D}{(b-a)}\left[a\left(\frac{r_o}{r}\right)^b - b\left(\frac{r_o}{r}\right)^a\right], \qquad (1)$$

where D and r_o — depth and coordinate of the potential minimum, $b > a > 1$ — numerical parameters, r — distance between atom centers.

If we apply the „only nearest neighbor's interaction" approximation and use the Einstein model for the crystal vibrational spectrum, then for the specific (per atom) Helmholtz free energy of the crystal, we may take the expression:

$$f_H(k_n, R, T) = \left(\frac{k_n}{2}\right) D \cdot U(R) + 3k_B\Theta_E(k_n, R) \times \left\{\frac{1}{2} + \left(\frac{T}{\Theta_E(k_n, R)}\right)\ln\left[1 - \exp\left(-\frac{\Theta_E(k_n, R)}{T}\right)\right]\right\} - \frac{\chi_{el}}{2N_A}\left(\frac{v}{v_o}\right)^{\gamma_{el}} T^2. \qquad (2)$$

Here $k_B = 1.3807 \cdot 10^{-23}$ J/K — Boltzmann constant, k_n — first coordination number, Θ_E — Einstein temperature associated with Debye temperature by the ratio [17] $\Theta = (4/3)\Theta_E$, $R = r_o/c$ — relative linear density of the crystal, $c = (6k_p v/\pi)^{1/3}$ — distance between the centers of the nearest atoms, k_p — structure packing index, $v = V/N$ — specific volume, V and N — volume and number of the crystal atoms,

$$v_o = \frac{\pi r_o^3}{6k_p}, \quad U(R) = \frac{aR^b - bR^a}{b-a}.$$

In contrast to the method in [14–16], here, we took into account the contribution of ELS. Therefore, the last term in the expression (1) determines the contribution of ELS, which is especially noticeable for the refractory metals [18–20]. In this term $N_A = 6.022 \cdot 10^{23}\,\mathrm{mol}^{-1}$ — Avogadro's number, χ_{el} — coefficient of electron heat capacity, which is determined from measurements of the heat capacity at low temperatures, γ_{el} — the electron Grüneisen parameter.

Assuming that the values χ_{el} and γ_{el} — do not depend on the density of the crystal, from the expression (2) for the equation of state (P) and the isothermal elastic modulus (B_T), the expressions can be obtained

$$P(k_n, R, T) = -\left(\frac{\partial f_H}{\partial v}\right)_T = P_{lat} + \gamma_{el}\frac{\chi_{el}}{2N_A v_o}\left(\frac{v}{v_o}\right)^{\gamma_{el}-1} T^2 = \left[\frac{k_n}{6} D \cdot U'(R) + 3k_B\Theta_E \cdot \gamma \cdot E_w\left(\frac{\Theta_E}{T}\right)\right]\frac{1}{v} + \gamma_{el}\frac{\chi_{el}}{2N_A v_o}\left(\frac{v}{v_o}\right)^{\gamma_{el}-1} T^2, \qquad (3)$$

$$B_T(k_n, R, T) = -v\left(\frac{\partial P}{\partial v}\right)_T = B_{Tlat} + \gamma_{el}(1-\gamma_{el})\frac{\chi_{el}}{2N_A v_o} \times \left(\frac{v}{v_o}\right)^{\gamma_{el}-1} T^2 = P_{lat} + \left[\frac{k_n}{18} D \cdot U''(R) + 3k_B\Theta_E \times \gamma(\gamma - q) \cdot E_w\left(\frac{\Theta_E}{T}\right) - 3k_B \cdot \gamma^2 \cdot T \cdot F_E\left(\frac{\Theta_E}{T}\right)\right]\frac{1}{v} + \gamma_{el}(1-\gamma_{el})\frac{\chi_{el}}{2N_A v_o}\left(\frac{v}{v_o}\right)^{\gamma_{el}-1} T^2. \qquad (4)$$

Here γ and q — the first and second lattice parameters of Grüneisen, and the last terms in (3) and (4) determine the contribution of ELS to these functions,

$$E_w(y) = 0.5 + \frac{1}{[\exp(y) - 1]}, \quad F_E(y) = \frac{y^2\exp(y)}{[\exp(y) - 1]^2},$$

$$U'(R) = R\left[\frac{\partial U(R)}{\partial R}\right] = \frac{ab\left(R^b - R^a\right)}{b-a},$$

$$U''(R) = R\left[\frac{\partial U'(R)}{\partial R}\right] = \frac{ab\left(bR^b - aR^a\right)}{b-a}. \qquad (5)$$

Within the framework of „only nearest-neighbor interaction" approximation, the expression was obtained for the Debye temperature of the single-component crystal [21]

$$\Theta(k_n, R) = A_w(k_n, R)\,\xi\left[-1 + \left(1 + \frac{8D}{k_B A_w(k_n, R)\,\xi^2}\right)^{1/2}\right]. \qquad (6)$$

Here, the function A_w arises due to taking into account the energy of „zero vibrations“ of atoms in a crystal and has the following form:

$$A_w(k_\mathrm{n}, R) = K_R \frac{5k_\mathrm{n} a b(b+1)}{144(b-a)} R^{b+2},$$

$$K_R = \frac{\hbar^2}{k_\mathrm{B} r_\mathrm{o}^2 m}, \quad \xi = \frac{9}{k_\mathrm{n}}. \tag{7}$$

where m — atomic mass, $\hbar = 1.0546 \cdot 10^{-34}\,\mathrm{J}\cdot\mathrm{s}$ — Planck constant.

From Eq. (6) it is easy to find expressions for the first (γ) and second (q) Grüneisen parameters, which have the form

$$\gamma = -\left(\frac{\partial \ln\Theta}{\partial \ln v}\right)_T = \frac{b+2}{6(1+X_w)}, \tag{8}$$

$$q = \left(\frac{\partial \ln\gamma}{\partial \ln v}\right)_T = \gamma \frac{X_w(1+2X_w)}{(1+X_w)}, \tag{9}$$

Here, the function $X_w = A_w\xi/\Theta$ determines the role of quantum effects in calculating the Grüneisen lattice parameters.

Since the Debye temperature from (6) does not depend on the temperature during isochoric heating, assuming that the values χ_el and γ_el are independent of temperature, from the Eq. (2) for the molar isochoric heat capacity, we can obtain the expression

$$C_v(k_\mathrm{n}, R, T) = 3N_\mathrm{A}k_\mathrm{B}\cdot F_\mathrm{E}\left(\frac{\Theta_\mathrm{E}}{T}\right) + \chi_\mathrm{el}\left(\frac{v}{v_\mathrm{o}}\right)^{\gamma_\mathrm{el}} T, \tag{10}$$

where the first term determines the lattice isochoric heat capacity ($C_{v\,\mathrm{lat}}$), and the second is the contribution of ELS to the isochoric heat capacity ($C_{v\,\mathrm{el}}$).

The isobaric thermal volume-expansion coefficient can be calculated from the Grüneisen equation [17,18,22]:

$$\alpha_p(k_\mathrm{n}, R, T) = \frac{1}{v}\left(\frac{\partial v}{\partial T}\right)_P = \frac{\gamma\cdot C_{v\,\mathrm{lat}}}{V\cdot B_{T\,\mathrm{lat}}} + \frac{\gamma_\mathrm{el}\cdot C_{v\,\mathrm{el}}}{V\cdot B_T}$$

$$= \frac{\gamma\cdot C_{v\,\mathrm{lat}}}{N_\mathrm{A} v_\mathrm{o} B_{T\,\mathrm{lat}}}\left(\frac{v_\mathrm{o}}{v}\right) + \frac{\gamma_\mathrm{el}\cdot\chi_\mathrm{el}}{N_\mathrm{A} v_\mathrm{o} B_T}\left(\frac{v_\mathrm{o}}{v}\right)^{1-\gamma_\mathrm{el}} T, \tag{11}$$

The molar isobaric heat capacity is defined as the sum of the lattice and electron isobaric heat capacities expressed as

$$C_p = C_{p\,\mathrm{lat}} + C_{p\,\mathrm{el}}$$

$$= C_{v\,\mathrm{lat}}\left(1+\gamma\cdot\alpha_{p\,\mathrm{lat}}\cdot T\right) + C_{v\,\mathrm{el}}\left(1+\gamma_\mathrm{el}\cdot\alpha_{p\,\mathrm{el}}\cdot T\right). \tag{12}$$

The obtained expressions (2)–(12) allow to calculate the equation of state and thermodynamic properties versus normalized volume $v/v_\mathrm{o} = (c/r_\mathrm{o})^3 = R^{-3}$ and temperature of the single-component crystal with such structure (i. e. at given values k_n and k_p), when parameters of interatomic potential (1) and ELS parameters of the crystal: χ_el and γ_el are known.

Several methods have been proposed to determine the value of γ_el. For example, [18–20] $\gamma_\mathrm{el} = 2/3$ is obtained from the model of the ideal degenerate electron gas. From Thomas–Fermi model it follows [19,20] $\gamma_\mathrm{el} = 1/2$. More complex methods have also been proposed for calculating the values γ_el reviewed in papers [19,20]. However, the functions γ_el obtained in these methods include the adjusting constants, the physical meaning of which is difficult to determine. Experimental estimates of the value γ_el from the ratio [22] were also carried out at low temperatures: $\gamma_\mathrm{el} = VB_T\alpha_{p\,\mathrm{el}}/C_{v\,\mathrm{el}}$. In these studies, the values for the refractory metals were obtained: $\gamma_\mathrm{el} = 1.3\,(\mathrm{Ta}) - 3.5\,(\mathrm{Re}) > 1$. However, from the expression (4) we may see that at $\gamma_\mathrm{el} > 1$ we get $B_{T\,\mathrm{el}} < 0$. This indicates that such electron subsystem is unstable. Therefore, in order to evaluate the contribution by the electron subsystem to different properties of the metal we take $\gamma_\mathrm{el} = 2/3$.

To calculate the surface properties of both macro-, and nanocrystal we developed the RP-model [14,16], which uses the potential of pair interatomic interaction (1). In RP-model, the specific surface energy was calculated by varying the specific free energy of a nanocrystal with an infinitesimal change in the shape of its surface. In case of using the ideal electron gas model, the value of f_el from (2) will not depend on the shape of the surface of the nanocrystal. Therefore, contributions of ELS will not be included in the expression for the specific surface energy (σ) of a nano- or macrocrystal. However, since the value of σ is related to the thermodynamic properties of the crystal, its baric and temperature dependences can change when ELS is taken into account. Thus, for the specific surface energy of a macrocrystal facet (100) its isochoric and isobaric derivatives in temperature and derivative σ in specific surface area, we use the following expressions obtained in [14–16]:

$$\sigma(k_\mathrm{n}, R, T) = -\frac{k_\mathrm{n} D R^2}{12\alpha^{2/3} r_\mathrm{o}^2}\Big[U(R) + 3H_w(R, T)\Big], \tag{13}$$

$$\sigma'(T)_v = \left(\frac{\partial\sigma}{\partial T}\right)_v = -\frac{3k_\mathrm{B}R^2\gamma}{2\alpha^{2/3}(b+2)r_\mathrm{o}^2} F_\mathrm{E}\left(\frac{\Theta_\mathrm{E}}{T}\right), \tag{14}$$

$$\sigma'(T)_P = \left(\frac{\partial\sigma}{\partial T}\right)_P = \sigma'(T)_v + v\cdot\alpha_p\left(\frac{\partial\sigma}{\partial T}\right)_T$$

$$= \sigma'(T)_v - \frac{2}{3}\sigma\cdot\alpha_p\cdot\Delta_p, \tag{15}$$

Table 1. Properties of BCC-Ta at $P=0$ and $T=300\,\mathrm{K}$

Property	$v=V/N$, Å^3/atom	α_p, $10^{-6}\mathrm{K}^{-1}$	B_T, GPa	$B'(P)=(\partial B_T/\partial P)_T$	Θ, K	γ
$\chi_{el}=0$	18.0353	18.644	174.75	5.1345	261.42	1.46987
χ_{el} through (19)	18.0363	19.111	174.70	5.1348	261.40	1.46987
Data from experimental and theory (in brackets) papers of other authors	18.020 [2,28], 18.0417 [4], 18.035 [5,29], 18.019 [6,28], (18.47) [7], (18.089) [13], (18.255) [19], 18.046 [30]	18–19.8 [3], 19.5 [4], 19.8 [7,18], 18–21.5, (19.54) [9], (19.74) [29]	197.9(3.7) [2,27], 187–216 [4], 196.1 [6,28], (194.4) [7], 191.1(3) [11], (191) [29], 179.60(2.18) [30]	3.17(10) [2,27], 2.5–4.3 [4], 3.64 [6,28], (3.06) [7], 4.006(2) [11], (3.83–4.08) [29]	263.8 [3], 229, (220) [7], 215–264.5 [9], 222–263.8 [10], 240 [18], 225 [19]	1.639 [4], 1.65, (1.75) [7], 1.69 [19], 1.5–1.7 [22], (1.658) [29]

The first two lines show the values calculated with parameters of potential from (18): in the first line — neglecting ELS, i.e. at $\chi_{el}=0$, and in the second line — at $\chi_{el}=4.36\,\mathrm{mJ/(mol\,K^2)}$ [27]. Below are given experimental and theoretical (in brackets) data of other authors

$$\Delta_p = -\left[\frac{\partial \ln(\sigma)}{\partial \ln(\Sigma/N)}\right]_T = -\frac{1}{2}\left[\frac{\partial \ln(\sigma)}{\partial \ln(c)}\right]_T = -\frac{3}{2}\left[\frac{\partial \ln(\sigma)}{\partial \ln(v/v_o)}\right]_T = 1+\frac{U'(R)-\left[q-\gamma\cdot t_y\left(\frac{\Theta_E}{T}\right)\right]9H_w(R,T)}{2\left[U(R)+3H_w(R,T)\right]}, \quad (16)$$

Here Σ — crystal surface area, $\alpha=\pi/(6k_p)$,

$$H_w(R,T)=\frac{6\gamma}{b+2}\frac{k_B\Theta_E}{Dk_n}E_w\left(\frac{\Theta_E}{T}\right),$$

$$t_y(y)=1-\frac{2y\exp(y)}{\left[\exp(2y)-1\right]}. \quad (17)$$

We can easily see that when $T\to 0\,\mathrm{K}$ the functions of (14) and (15) tend to zero at any value of the density R, which complies with the third law of thermodynamics. Note that the expressions (2)–(17) do not take into account either vacancies or self-diffusion of atoms, because, as shown in [23–25], their influence becomes negligible when the crystal is compressed.

3. Tantalum thermoelastic properties

3.1. Determination of the interatomic potential parameters

We know that tantalum (Ta, $m(\mathrm{Ta})=180.948$ a.m.u.; $Z=73$; [Xe]$4f^{14}5d^36s^2$) has a body-centered cubic (BCC) structure ($k_n=8$, $k_p=0.6802$), and is free from any polymorphous phase transitions up to 300 GPa [12]. For BCC-Ta, the parameters of the paired interatomic potential (1) were initially determined by the method described in [14]. However, the values r_o, D, b and a obtained for BCC-Ta in this way didn't provide a good dependence for the equation of state $P(v, T)$. Therefore, a new method of determination of the interatomic potential parameters (1) was used in the present study. This method was presented and tested for rhodium in [26]. Thus, using this method for BCC-Ta the following values of pair interatomic potential (1) were obtained:

$$r_o=2.8558\cdot 10^{-10}\,\mathrm{m}, \quad D/k_B=30142.59\,\mathrm{K},$$

$$b=6.83, \quad a=2.54. \quad (18)$$

The value χ_{el}, which is determined from the temperature dependence of the heat capacity at low temperatures, has been measured for tantalum in many studies, a review of which is presented in [10,18,27]. Yet, the value χ_{el} was found in the experiment with such an accuracy that the estimates known from the literature lie within [10], $\chi_{el}(\mathrm{Ta})=3.35-6.28\,\mathrm{mJ/(mol\,K^2)}$. From the mentioned papers we took the value obtained in [27]. Thus, to calculate the contributions of ELS into the properties of BCC-Ta we use the following values:

$$\gamma_{el}=2/3, \quad \chi_{el}=4.36\,\mathrm{mJ/(mol\,K^2)}\ [27]. \quad (19)$$

Table 1 shows BCC-Ta properties calculated, using parameters from (18) and (19) at $P=0$ and $T=300\,\mathrm{K}$.

As can be seen from Table 1, the agreement between the calculated data and the experimental and theoretical (in brackets) estimates of the other authors is quite good. It should be stressed, however, that the values B_T and $B'(P)=(\partial B_T/\partial P)_T$ were determined experimentally not in point $P=0$, but by adjusting the dependence $P(v/v_o)$ measured in some interval for the three-parameter equation of state: either a third-order Birch–Murnaghan equation or Rydberg–Vinet equation [28].

3.2. State equation

Figure 1 illustrates the isotherms of BCC-Ta equation of state: left-hand for 300 K, right-hand for 3000 K. The pressure is in GPa, while the specific volume is

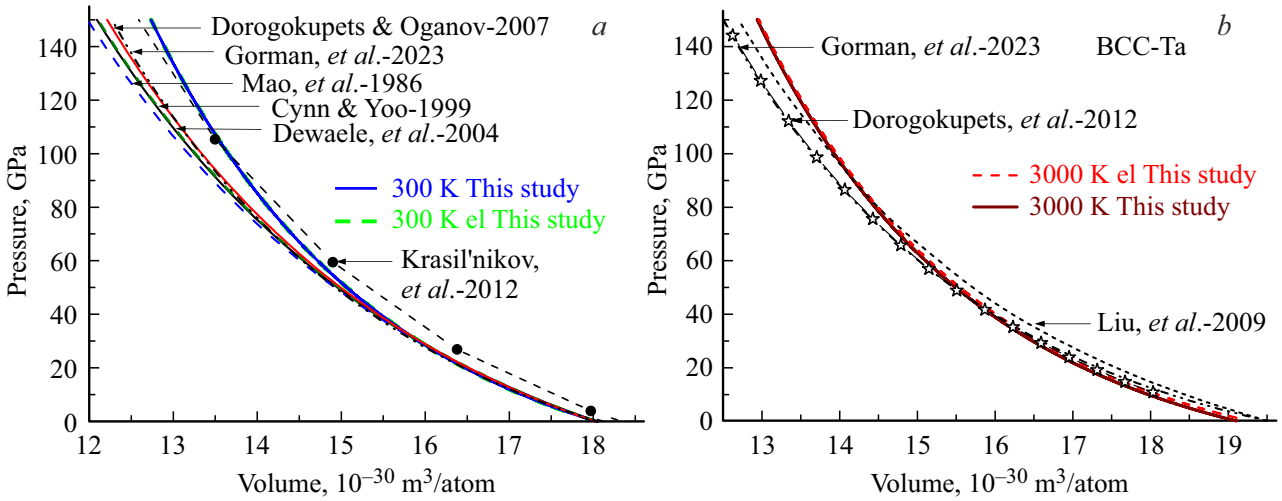

Figure 1. Equation of state BCC-Ta: *a*) for 300 K, *b*) for 3000 K. Solid line and dashed line — our calculations for isotherms neglecting ELS (solid) and taking into account ELS (dashed). At this scale, these lines merge. Other lines describe the findings from papers [2,4–6,8,28–30].

in $Å^3/atom = 10^{-30}\,m^3/atom$. Solid line and dashed line — our calculations for isotherms neglecting ELS (solid) and taking into account ELS (dashed), respectively. At this scale, these lines merge.

Experimental data for the isotherm $P(v)$ are usually approximated by various three-parameter dependencies. The third-order Birch–Murnaghan equation was often used [4]:

$$P(v) = \frac{3}{2} B_{0T} \left[\left(\frac{v}{v_o} \right)^{-7/3} - \left(\frac{v}{v_o} \right)^{-5/3} \right] \times \left\{ 1 - \frac{3}{4} \left(4 - B_0' \right) \cdot \left[\left(\frac{v}{v_o} \right)^{-2/3} - 1 \right] \right\}. \quad (20)$$

Also Rydberg–Vinet equation was used [2,5,6,28] having the following form:

$$P(v) = 3B_{0T} \left(\frac{v}{v_o} \right)^{-2/3} \left[1 - \left(\frac{v}{v_o} \right)^{1/3} \right] \times \exp\left\{ 1.5 \left(B_0' - 1 \right) \cdot \left[1 - \left(\frac{v}{v_o} \right)^{1/3} \right] \right\}. \quad (21)$$

Recently, a modified five-parameter Vinet equation has been proposed in [30] expressed as follows

$$P(v) = 3B_{0T} \left(\frac{v}{v_o} \right)^{-2/3} \left[1 - \left(\frac{v}{v_o} \right)^{1/3} \right] \times \exp\left\{ \eta \cdot \left[1 - \left(\frac{v}{v_o} \right)^{1/3} \right] + \beta \cdot \left[1 - \left(\frac{v}{v_o} \right)^{1/3} \right]^2 + \psi \cdot \left[1 - \left(\frac{v}{v_o} \right)^{1/3} \right]^3 \right\}. \quad (22)$$

Figure 1 shows the dependence for equation (20) along isotherm 300 K with parameters from [4]:

$$v_o = 18.0417\,Å^3/atom, \quad B_{0T} = 194.7\,GPa, \quad B_0' = 3.4.$$

For the equation (21) at 300 K the following parameters were used:

$v_o = 18.020\,Å^3/atom$, $B_{0T} = 197.9$ GPa, $B_0' = 3.17$ from [2,28]

$v_o = 18.035\,Å^3/atom$, $B_{0T} = 197.0$ GPa, $B_0' = 3.39$ from [5],

$v_o = 18.019\,Å^3/atom$, $B_{0T} = 196.1$ GPa, $B_0' = 3.64$ from [6,28].

For equation (22) we used parameters obtained in [30]:

for 298 K: $v_o = 18.046\,Å^3/atom$, $B_{0T} = 179.60(2.18)$ GPa, $\eta = 4.68(0.16)$, $\beta = -0.22(0.72)$, $\psi = 10.08(1.03)$

for 3000 K: $v_o = 19.492\,Å^3/atom$, $B_{0T} = 128.67(1.81)$ GPa, $\eta = 5.46(0.18)$, $\beta = -2.20(0.73)$, $\psi = 11.75(0.98)$.

Also in Figure 1, *a* the results from [8] (solid circles) are shown obtained by the electron density functional method at $T = 0$ K. Figure 1, *b* shows the results calculated for the isotherm $T = 3000$ K in [7] (dashed line), [29] (open asterisks) and [30] (dotted line with two dots). At this scale, dependencies from [29,30] merge. As can be seen from Figure 1, the effect of ELS on the equation of state in the studied range of $P-T$ parameters is very small.

3.3. Isothermal elastic modulus

Figure 2 shows the pressure (left) and temperature (right) dependences of the isothermal elastic modulus (B_T, in GPa) of BCC-Ta. Solid line and dashed line —

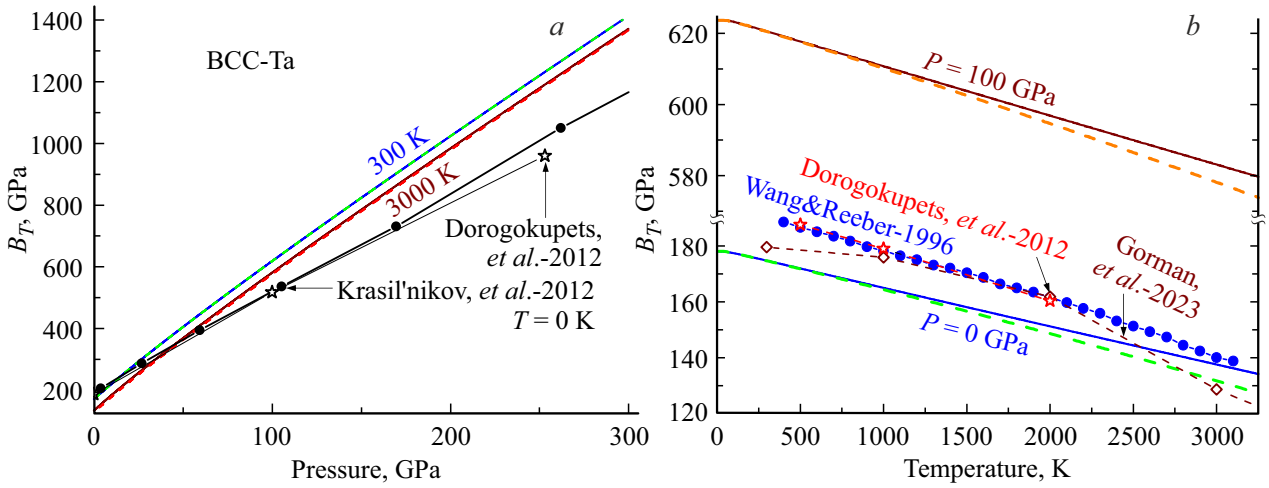

Figure 2. *a*) Pressure and *b*) temperature dependences of the isothermal elastic modulus of BCC-Ta. Solid line and dashed line — our calculations neglecting ELS (solid) and taking into account ELS (dashed). In the left-hand graph these dependencies merge. Other lines describe the results from the studies [8,29–31].

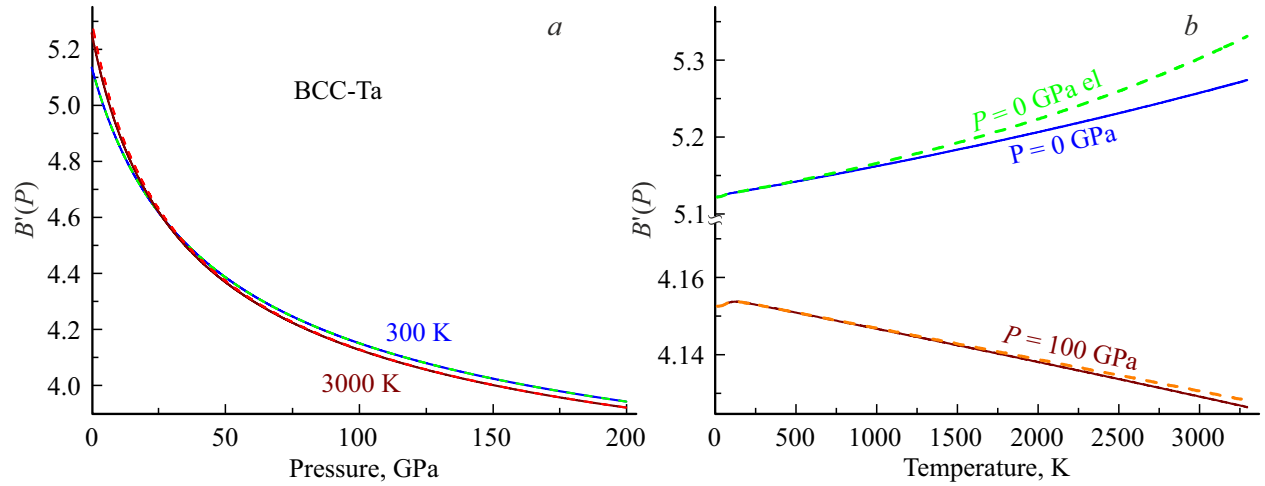

Figure 3. *a*) Pressure and *b*) temperature dependences of the derivative elastic modulus with respect to pressure for BCC-Ta. Solid line and dashed line — our calculations neglecting ELS (solid) and taking into account ELS (dashed).

our calculations neglecting ELS (solid) and taking into account ELS (dashed). Other lines describe the results from [8,29–31]. As can be seen from Figure 2, the effect of ELS on the isothermal baric dependences of the elastic modulus of BCC-Ta is insignificant. However, as can be seen from the right graph, taking into account ELS leads to a decrease in the value of B_T, and with an increase in temperature, the influence of ELS rises. As can be seen from Figure 2, the function B_T varies almost linearly both along the isotherm and along the isobar.

Figure 3 illustrates pressure $(3,a)$ and temperature $(3,b)$ dependencies of the derivative of the elastic modulus with respect to pressure $(B'(P)=(\partial B_T/\partial P))$ for BCC-Ta. As can be seen from Figure $3,a$, the isotherms $B'(P)$ are weakly dependent on ELS with isothermal pressure increase. However, with an isobaric increase in temperature, when taking into account ELS, the value $B'(P)$ rises slightly. At a certain pressure (P_x), the isotherms $B'(P)$ intersect. BCC-Ta will have the following coordinates of isotherms $B'(P)$ intersection points:

$$P_x = 26.684\,\text{GPa},\ B'(P)_x = 4.598 - \text{excluding ELS},$$

$$P_x = 33.742\,\text{GPa},\ B(P)_x = 4.522 - \text{including ELS}.$$

At a pressure of P_x, the function $B'(P)$ does not change with an isobaric increase in temperature. At $P > P_x$, the function $B'(P)$ decreases with an increase in temperature along the isobar, and at $P < P_x$, the function $B'(P)$ rises with an isobaric increase in temperature, as shown in Figure $3,b$.

3.4. Thermal expansion coefficient

Figure 4 shows the pressure $(4,a)$ and temperature $(4,b)$ dependencies of the thermal expansion coefficient $(\alpha_p,$

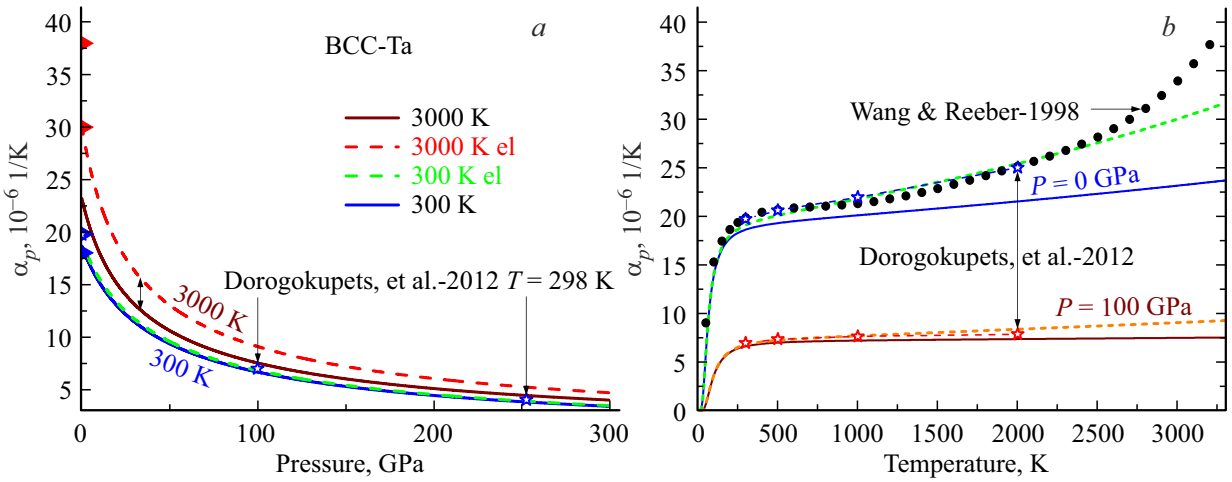

Figure 4. *a*) Pressure and *b*) temperature dependencies of the thermal expansion coefficient of BCC-Ta. Solid line and dashed line — our calculations neglecting ELS (solid) and taking into account ELS (dashed). In the left-hand graph at $T = 300$ K these dependencies merge. The symbols on the vertical axis of the left-hand graph show the spread of experimental data at $P = 0$ GPa for $T = 300$ K (lower) and $T = 3000$ K (upper) and studies [3,9]. Asterisks denote the results from [29]: *a*) for $T = 298$ K, *b*) upper — for $P = 0$ GPa, lower — at $P = 100$ GPa.

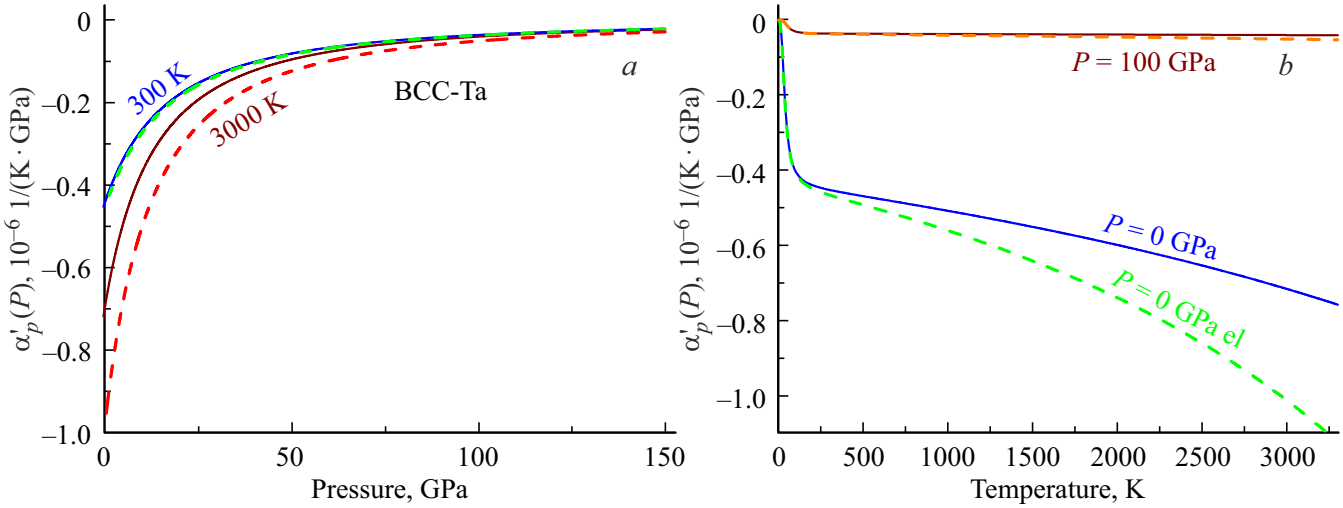

Figure 5. *a*) Pressure and *b*) temperature dependencies of the thermal expansion coefficient derivative with respect to pressure for BCC-Ta. Solid line and dashed line — our calculations neglecting ELS (solid) and taking into account ELS (dashed).

in 10^{-6} 1/K) of BCC-Ta. Solid line and dashed line — our calculations neglecting ELS (solid) and taking into account ELS (dashed). In the left-hand graph at $T = 300$ K these dependencies merge. However, taking into account ELS leads to an increase in α_p, and with an increase in temperature, this growth intensifies markedly. As can be seen from Figure 4, when taking into account ELS, the agreement with experimental data from [3,9] is noticeably improved. As pressure grows the value α_p goes down, which is consistent with findings from [6,7,13,29].

Figure 5 illustrates the pressure $(5, a)$ and temperature $(5, b)$ dependencies of the thermal expansion coefficient with respect to pressure $(\alpha'_p(P) = (\partial\alpha_p/\partial P)_T$, in 10^{-6} 1/(GPa K)) for BCC-Ta. Solid line and dashed line — our calculations neglecting ELS (solid) and taking into account ELS (dashed). Figure 5 shows that ELS accounting is most noticeable at low pressures and high temperatures, and it is also seen that the function $\alpha'_p(P)$ weakly depends on the temperature along the isobar at $P > 100$ GPa.

3.5. Isobar heat capacity

Figure 6 illustrates pressure $(6, a)$ and temperature $(6, b)$ dependencies of the normalized isobar heat capacity for BCC-Ta: $C_p/(Nk_B)$. Solid line and dashed line — our calculations neglecting ELS (solid) and taking into account ELS (dashed). The symbols in Figure 6, *b* show

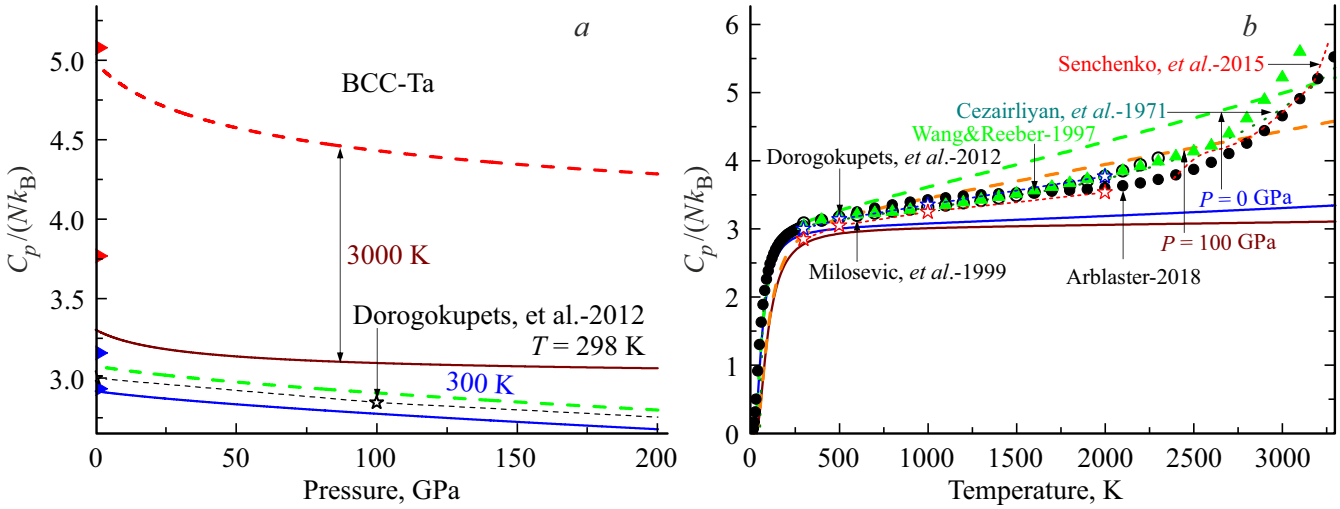

Figure 6. *a*) Pressure and *b*) temperature dependencies of the normalized isobaric thermal capacity of BCC-Ta. Solid line and dashed line — our calculations neglecting ELS (solid) and taking into account ELS (dashed). The symbols on the vertical axis of the left-hand graph show the spread of experimental data at $P = 0$ GPa for $T = 300$ K (lower) and $T = 3000$ K (upper) and [9]. The symbols on the right graph show experimental results from [10] — solid circles, [31] — solid triangles, [32] — open large circles. Asterisks denote the results from [29]: *a*) for $T = 298$ K, *b*) upper — for $P = 0$ GPa, lower — at $P = 100$ GPa. The thin dotted line shows the experimental results from [1], the dashed line shows the experimental results from [33], approximated by the function (23).

experimental results from the studies [10] — solid circles, [31] — solid triangles, [32] — open large circles. Asterisks denote the results from [29]: in Figure 6, *a* for $T = 298$ K, in Figure 6, *b* upper for $P = 0$ GPa, lower for $P = 100$ GPa. The thin dotted line shows the experimental results from [1], the dashed line shows the experimental results from [33], approximated by the function

$$\frac{C_p(T)}{k_B N_A} = 3 - \frac{5869.382}{T^2} + 3.1151 \cdot 10^{-4} T + 3.4278 \cdot 10^{-18} T^5. \quad (23)$$

As can be seen from Figure 6, when taking into account ELS, the agreement with experimental data from [1,9,10,31–33] is noticeably improved. As pressure grows the value C_p goes down, which is consistent with findings from [6,7,13,29].

On Figure 7 shows the pressure $(7, a)$ and temperature $(7, b)$ dependences of the pressure derivative of the normalized isobaric heat capacity $(C'_p(P)/(Nk_B) = (Nk_B)^{-1}(\partial C_p/\partial P)_T$, in GPa^{-1}) for BCC-Ta. Solid line and dashed line — our calculations neglecting ELS (solid) and taking into account ELS (dashed). As can be seen from Figure 7, *b*, the function $C'_p(P)$ on the isobar has a minimum and a maximum, which are located at points

$T_{\min} = 59.6$ K and $C'_p(P)_{\min}/(Nk_B) = -0.0168\ \mathrm{GPa}^{-1}$ for $P = 0$ GPa,

$T_{\min} = 86.6$ K and $C'_p(P)_{\min}/(Nk_B) = -0.0048\ \mathrm{GPa}^{-1}$ for $P = 100$ GPa.

Here, the coordinates of the minima do not depend on accounting ELS.

$T_{\max} = 519.1\ K$ and $C'_p(P)_{\max}/(Nk_B) = -0.0017\ \mathrm{GPa}^{-1}$ for $P = 0$ GPa,

$T_{\max} = 413.3\ K$ and $C'_p(P)_{\max}/(Nk_B) = -0.0026\ \mathrm{GPa}^{-1}$ for $P = 0$ GPa + el,

$T_{\max} = 1062.3\ K$ and $C'_p(P)_{\max}/(Nk_B) = -0.0002\ \mathrm{GPa}^{-1}$ for $P = 100$ GPa,

$T_{\max} = 668.2\ K$ and $C'_p(P)_{\max}/(Nk_B) = -0.0006\ \mathrm{GPa}^{-1}$ for $P = 100$ GPa + el,

Here, the second lines show the results obtained when accounting for ELS.

3.6. Product $\alpha_p \cdot B_T$

In 1952 Francis Birch in his article suggested that for silicates and oxides at high temperatures $(T > \Theta)$ the product $\alpha_p \cdot B_T$ doesn't depend on pressure [34], i. e.

$$\alpha_p B_T = \left(\frac{\partial P}{\partial T}\right)_v = \left(\frac{\partial s}{\partial v}\right)_T \cong \text{const}. \quad (24)$$

where $s = -(\partial f_H/\partial T)_v$ — specific crystal entropy.

Later, it was also noticed that for many minerals at high temperatures, the product $\alpha_p \cdot B_T$ does not depend on temperature [35]. Thus, despite its simplicity, the approximation (24) has been widely used, and it is sometimes also called „αB-rule (αB rule)“ [36].

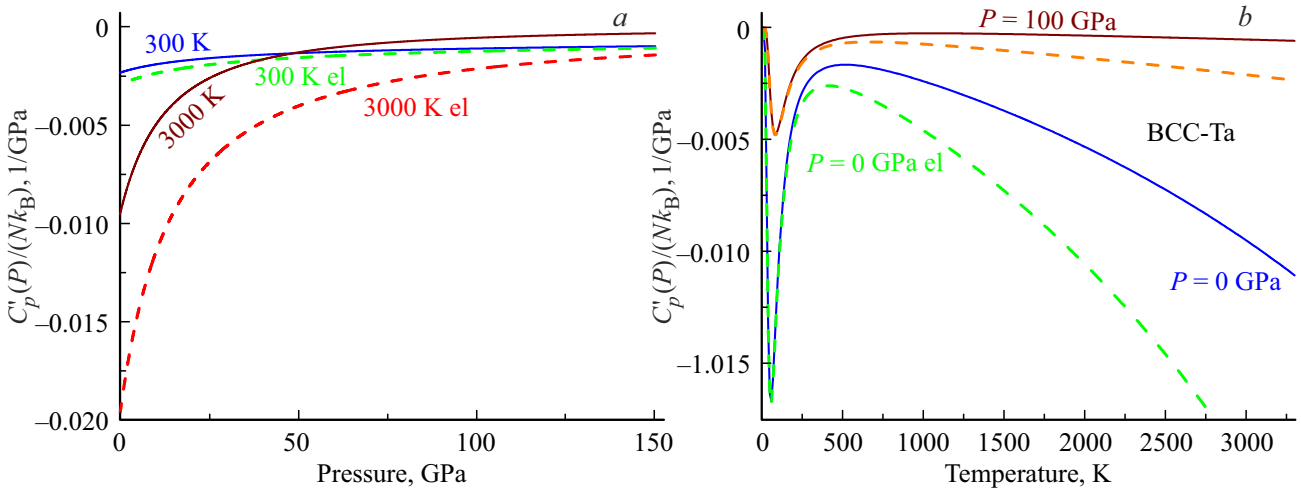

Figure 7. *a*) Pressure and *b*) temperature dependence of the pressure derivative of the normalized isobaric heat capacity for BCC-Ta. Solid line and dashed line — our calculations neglecting ELS (solid) and taking into account ELS (dashed). The function $C'_p(P)$ on an isobar has a minimum and a maximum.

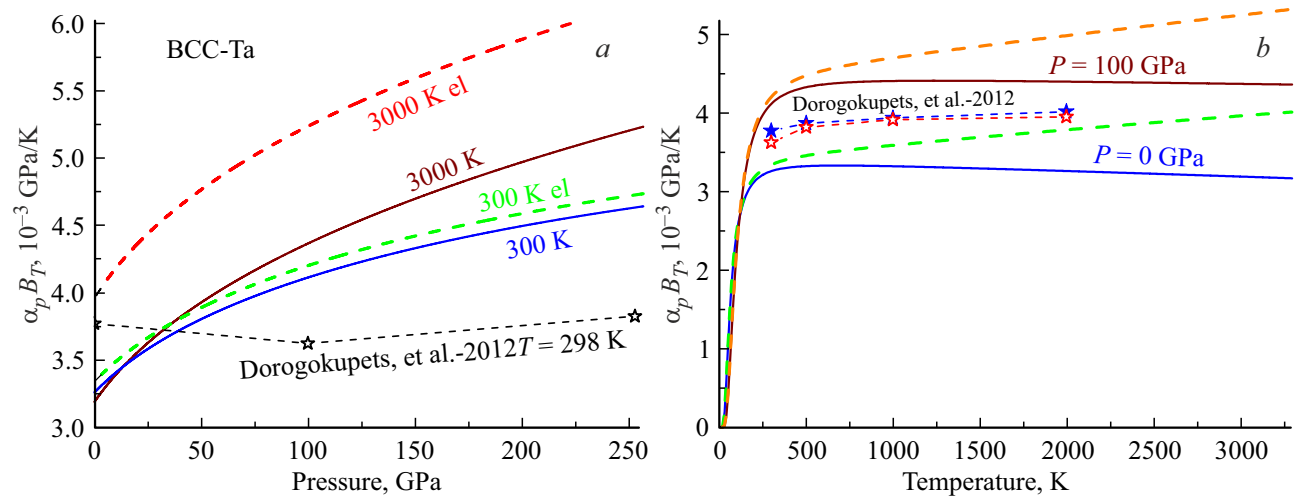

Figure 8. *a*) Pressure and *b*) temperature dependencies of the product of thermal expansion coefficient by the modulus of elasticity for BCC-Ta. Solid line and dashed line — our calculations neglecting ELS (solid) and taking into account ELS (dashed). Asterisks denote the results from [29]: *a*) for $T = 298$ K, *b*) solid asterisks — for $P = 0$, open — for $P = 100$ GPa.

Figure 8 shows pressure $(8, a)$ and temperature $(8, b)$ dependences of the product of the coefficient of thermal expansion by the elastic modulus ($\alpha_p \cdot B_T$, in 10^{-3} GPa/K) for BCC-Ta. Solid line and dashed line — our calculations neglecting ELS (solid) and taking into account ELS (dashed). As seen from Figure 8, *b*, at a certain temperature (T_B — Birch temperature) the isobars intersect. BCC-Ta will have the following coordinates of isobars intersection points:

$$T_B = 116.46\,\text{K},\ \ \alpha_p \cdot B_T = 2.68 \cdot 10^{-3}\,\text{GPa/K}$$
— excluding ELS,

$$T_B = 116.46\,\text{K},\ \ \alpha_p \cdot B_T = 2.72 \cdot 10^{-3}\,\text{GPa/K}$$
— including ELS.

At the Birch temperature, the function $\alpha_p \cdot B_T$ does not change with an isothermal increase in pressure. At $T < T_B$, the function $\alpha_p \cdot B_T$ declines with an increase in pressure along the isotherm, and at $T > T_B$, the function $\alpha_p \cdot B_T$ rises with an isothermal increase in pressure, as shown in Figure 8, *a*. For BCC-Ta T_B doesn't depend on whether ELS is accounted for or not. As can be seen from Figure 8, *b*, at $T > 400$ K the function $\alpha_p \cdot B_T$, neglecting ELS, decreases slightly with an isobaric increase in temperature. Yet, if ELS is taken into account, the function $\alpha_p \cdot B_T$ rises with the isobar temperature growth in $T > 400$ K. Therefore, in this case, the assumption that the product $\alpha_p \cdot B_T$ is independent of the temperature at $T > \Theta$ is not applicable. However, for BCC-Ta it is possible to select such value of $\chi_{\text{el}} < 4.36$ mJ/(mol K^2) in (19),

Table 2. Values of BCC-Ta surface properties, which are calculated when $P = 0$ and five temperatures. The first lines show the results obtained without taking into account ELS, and the second — taking into account ELS

T, K	v/v_o	$\sigma(100)$, 10^{-3} J/m^2	$-\sigma'(T)_v$, 10^{-6} J/(m^{2}K)	$-\sigma'(T)_P$, 10^{-6} J/(m^{2}K)	$\sigma'(P)_T$, 10^{-3} J/(m^{2}GPa)	$\Delta_p = -(\partial \ln\sigma/\partial \ln\Sigma)_T$
10	1.00186	4040.35	$\sim 10^{-4}$	$\sim 10^{-4}$	15.1607	1.00267
	1.00192	4040.19	$\sim 10^{-4}$	0.04	15.1674	1.00284
300	1.00601	4018.47	48.381	99.174	15.5875	1.01667
	1.00607	4018.31	48.3793	100.449	15.5939	1.01684
1000	1.01987	3946.27	49.521	105.405	16.8317	1.05575
	1.02066	3944.11	49.4958	110.169	16.9195	1.05788
2000	1.0413	3838.51	48.9561	110.327	18.8275	1.11281
	1.0450	3828.37	48.8411	121.714	19.265	1.12207
3200	1.06978	3702.36	48.1075	116.861	21.6587	1.18372
	1.0808	3672.23	47.7811	139.924	23.0778	1.20857

when the product $\alpha_p \cdot B_T$ will not depend on temperature at $T > \Theta$. However, would this method of determining the value of χ_{el} be correct?

4. Tantalum surface properties

4.1. Specific surface energy

Several different methods for calculating specific (per unit area) surface energy (σ) for a single-component substance crystal have been proposed to date (see, for example, [37–48]). Note that the specific surface energy for BCC-Ta has never been experimentally estimated. Such measurements are very labor-intensive, and they can only be carried out near the melting point of the crystal [49]. Therefore, the issue of the dependence of σ both on temperature and pressure at which the crystal is located is relevant. Table 2 shows the results of calculation of BCC-Ta surface properties using (13)–(17) and parameters of the potential from (18) at $P = 0$ and $T = 10$, 300, 1000, 2000, 3200 K.

The literature has a lot of estimates of the value of σ for the BCC-Ta facet (100). Below are some of them, obtained by using various methods of computation:

$\sigma(100)$, 10^{-3} J/m^2 = 2900 (0 K), 2680 (1773 K) [37],
2493 (T_m) [38], 3018 (298.2 K),
2270 (3269 K) [39], 2680 ± 500 (1773 K),
2480 ± 70 (2627–2787 K) [40],
3292 (0 K) [41], 3097 (0 K) [42],
2650 (T_m) [43], 4050 (0 K) [44],
3144–3150 (3290 K) [45], 3577 (3270 K) [46],
2270–3590 [47], 2740–3040 (0 K) [48].

Using the estimates from [37–39], we can obtain the average values of $(\Delta\sigma/\Delta T)_{P=0}$, which are in good agreement with our data for the isobaric derivative of σ in temperature:

$$(\Delta\sigma/\Delta T)_{P=0} = -(2900-2680)/1773 = -124.1 \cdot 10^{-6}\ \text{J/(m}^2\text{K)},\ \text{from 0–1773 K [37]},$$

$$(\Delta\sigma/\Delta T)_{P=0} = -(2900-2493)/3290 = -123.7 \cdot 10^{-6}\ \text{J/(m}^2\text{K)},\ \text{from 0–3290 K [37,38]},$$

$$(\Delta\sigma/\Delta T)_{P=0} = -(3018-2270)/2970.8 = -251.8 \cdot 10^{-6}\text{J/(m}^2\text{K)},\ \text{from 298.2–3269 K [39]},$$

$$\sigma'(T)_P = -170 \cdot 10^{-6}\ \text{J/(m}^2\text{K)},\ \text{defined by } T_m \text{ in [43]}.$$

As can be seen, the agreement between our calculations and the estimates of the other authors is quite good. However, the resulting value $(\Delta\sigma/\Delta T)_{P=0}$ is the average value over the specified temperature range. Meanwhile, as can be seen from Table 2, our calculated function $\sigma'(T)_P$ decreases non-linearly with temperature from $\sigma'(0\,\text{K})_P = 0$ to $\sigma'(T_m)_P < 0$.

There are no estimates of $\sigma'(P) = (\partial\sigma/\partial P)_T$ in the literature, so there's no information to compare our data from the table 2. Meanwhile, the dependence $\sigma(P)$ is necessary for studying both the crack initiation under the action of pressure on the crystal, and for obtaining the equation of state for the nanocrystal.

Figure 9, *a* shows the calculated pressure dependences of the specific surface energy (in 10^{-3} J/m^2) for the BCC-Ta facet (100) along the isotherms (top-down) 300 and 3000 K. It can be seen that at the certain pressure P_{max} the function $\sigma(P)$ reaches its maximum with the following

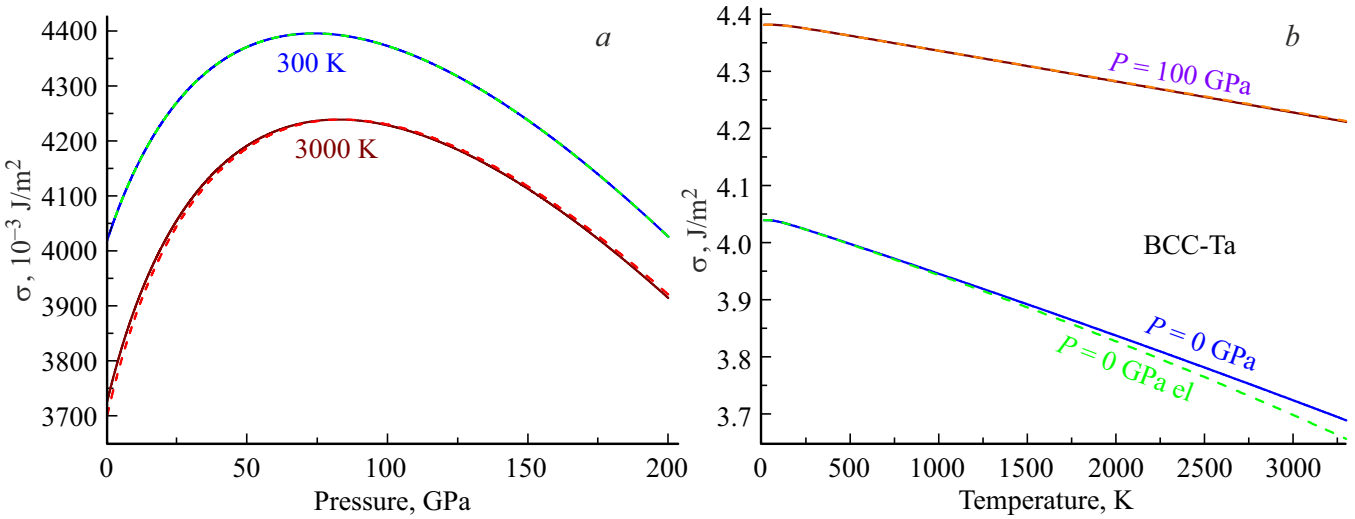

Figure 9. *a*) Pressure and temperature *b*) dependencies of the specific surface energy on facet (100) for BCC-Ta. Solid line and dashed line — our calculations neglecting ELS (solid) and taking into account ELS (dashed).

coordinates:

$T = 300$ K:

$\sigma_{\max} = 4395.2 \cdot 10^{-3}$ J/m^2 and $P_{\max} = 73.7$ GPa excluding and including ELS,

$T = 3000$ K:

$\sigma_{\max} = 4238.7 \cdot 10^{-3}$ J/m^2 and $P_{\max} = 83.1$ GPa excluding ELS,

$\sigma_{\max} = 4238.7 \cdot 10^{-3}$ J/m^2 and $P_{\max} = 83.7$ GPa including ELS.

Therefore, for BCC-Ta the coordinate of maximum of the function $\sigma(P)$ practically doesn't depend on whether ELS has been accounted for or not.

Figure 9, *b* shows the calculated temperature dependences of the specific surface energy (in 10^{-3} J/m^2) for the BCC-Ta facet (100) along the isobars 100 GPa (upper merging lines) and 0 GPa (lower lines). As can be seen from Figure 9, ELS accounting has little effect on the pressure and temperature dependences of the specific surface energy of BCC-Ta facet (100).

It can be seen in Figure 9 at certain compression $(v/v_o)_{fr} < 1$ (or when $P > P_{fr}$) the function $\sigma(v/v_o)$ transits into a negative domain. This behavior of the function $\sigma(v/v_o)$ when $v/v_o < (v/v_o)_{fr}$ shall induce fragmentation of the crystal, where the crystal will tend to increase its specific (per atom) inter-crystalline surface in any way. The effect of baric fragmentation was studied by us in more detail in the paper [50] on the example of crystals of neon, lithium and gold. For BCC-Ta for the normalized volume $(v/v_o)_{fr}$ and pressure P_{fr} in the fragmentation point (where $\sigma = 0$), with ELS taken into account and neglected, the following values were obtained:

$T = 300$ K: $(v/v_o)_{fr} = 0.50128$ and $P_{fr} = 757.295$ GPa excluding ELS,

$(v/v_o)_{fr} = 0.50128$ and $P_{fr} = 757.310$ GPa including ELS,

$T = 3000$ K: $(v/v_o)_{fr} = 0.50538$ and $P_{fr} = 749.915$ GPa excluding ELS,

$(v/v_o)_{fr} = 0.50538$ and $P_{fr} = 751.436$ GPa including ELS.

4.2. Derivatives of the surface energy with respect to the temperature

Figure 10, *a* shows the calculated pressure dependences of the derivative of the specific surface energy of the facet (100) with respect to the temperature $(\sigma'(T)_i = (\partial\sigma/\partial T)_i$, in 10^{-6} J/(m^{2}K)) along the isotherms (top-down) 300 and 3000 K. Solid growing lines — isobaric derivative $\sigma'(T)_P$, dashed declining lines — isochoric derivative $\sigma'(T)_v$. It can be seen that at the low pressures (i. e., when $P < 65-93$ GPa) the inequality $|\sigma'(T)_P| > |\sigma'(T)_v|$ is fulfilled. However, this inequality is reversed at the high pressures. Therefore, for the crystal, it is impossible to equate the isochoric and isobaric derivatives of the function σ with respect to the temperature as was done in some studies. It can be seen that for the function $\sigma'(T)_v$, taking into account ELS does not affect its pressure and temperature dependences.

Figure 10, *b* illustrates temperature dependencies of functions $\sigma'(T)_v$ and $\sigma'(T)_P$, calculated along the isobars 0 and 100 GPa. The function $\sigma'(T)_v$ at $P = 0$ GPa (upper line) is independent of ELS accounting, and at $T > 250$ K is practically independent of temperature. The function

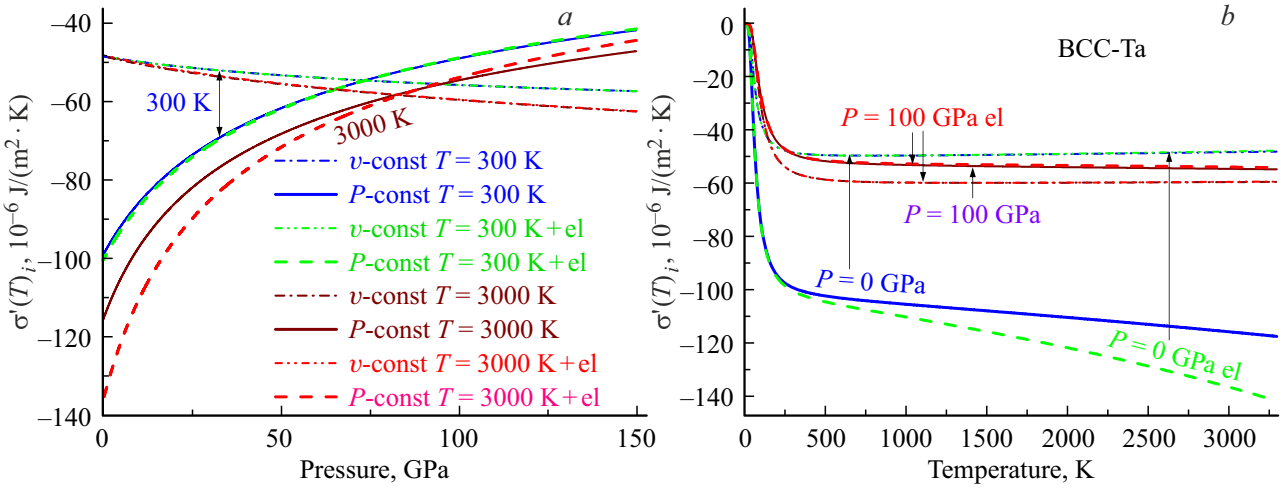

Figure 10. *a*) Baric and *b*) temperature dependences of the derivative of the specific surface energy of the facet (100) with respect to temperature for BCC-Ta. Solid line and dashed line — our calculations of function $\sigma'(T)_P$ neglecting ELS (solid) and taking into account ELS (dashed). Thin dotted lines — our calculations of the function $\sigma'(T)_v$ without taking into account ELS (with one dot) and with taking into account ELS (with two dots).

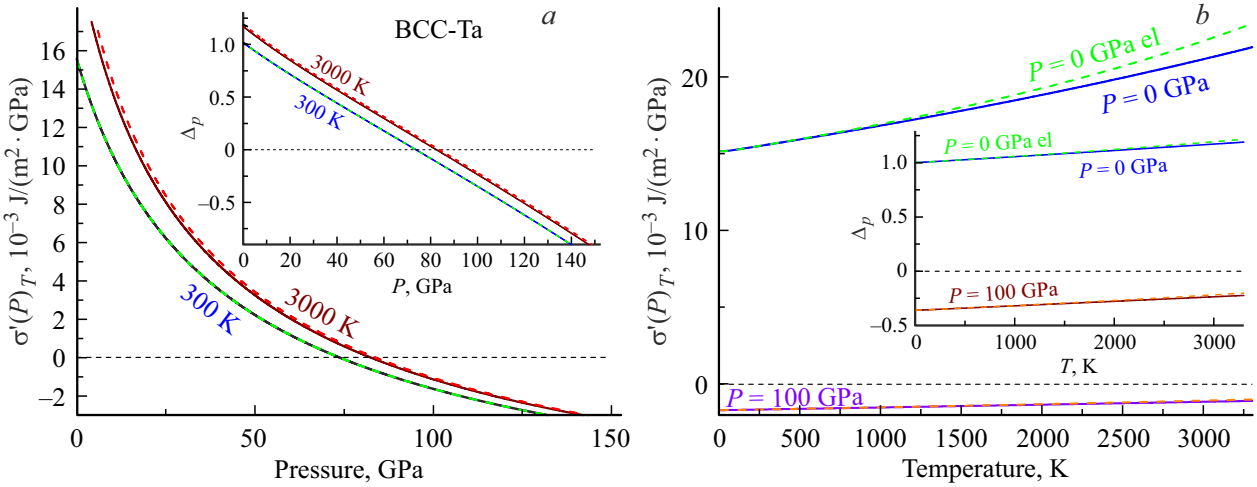

Figure 11. *a*) Pressure and *b*) temperature dependences of the derivative of the specific surface energy of the facet (100) with respect to pressure for BCC-Ta. Solid line and dashed line — our calculations neglecting ELS (solid) and taking into account ELS (dashed).

$\sigma'(T)_P$ at $P = 0$ GPa (lower lines) decreases (lower dashed line) when taking into account ELS, and its dependence on temperature rises. At $P = 100$ GPa the function $\sigma'(T)_v$ and function $\sigma'(T)_P$ do not depend on taking ELS into account: these functions merge.

4.3. Derivative of the surface energy with respect to the pressure

Figure 11 shows the calculated dependences of the derivative of the specific surface energy with respect to pressure ($\sigma'(P)_T = (\partial\sigma/\partial P)_T$, in 10^{-3} J/(m^{2}GPa)) for BCC-Ta. Figure 11, *a* shows the pressure dependences calculated along the isotherms (from bottom to top) 300 and 3000 K. Figure 11, *b* shows the temperature dependences calculated along the isobars (top-down) 0 and 100 GPa. It can be seen that when ELS is taken into account, the function $\sigma'(P)_T$ rises with temperature growth. However, with increasing pressure, accounting for ELS becomes irrelevant. The inserts show the baric (on the left) and temperature (on the right) dependences of the function $\Delta_p = -(\partial \ln\sigma/\partial \ln\Sigma)_T$ of (16) along the said functions of the temperature and the pressure. As can be seen from the graphs, the function Δ_p varies linearly both with isothermal increase of the pressure and with isobaric increase of the temperature. From Figure 11 we see that taking ELS into account has no any effect on the function $\Delta_p(P, T)$.

In Figures 3 and 11 we see the similarity of the pressure dependences of the derivative of isothermal elastic modulus with respect to pressure: $B'(P) = (\partial B_T/\partial P)_T$,

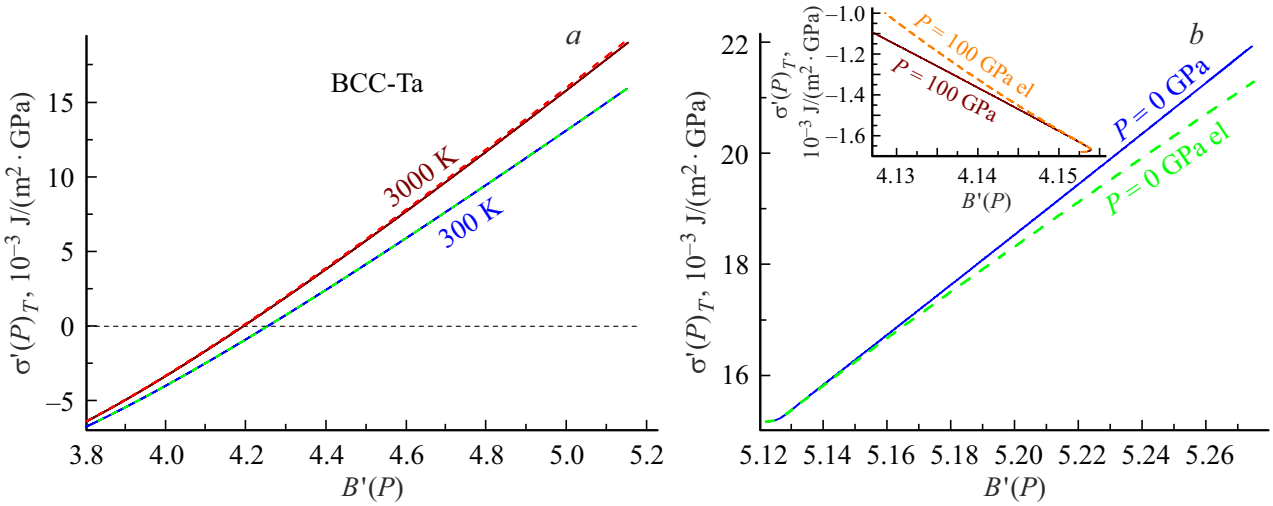

Figure 12. Derivatives of the specific surface energy with respect to pressure versus the derivative of the isothermal elastic modulus of BCC-Ta with respect to pressure. Pressure dependencies (a) are calculated along the isotherms (from bottom to top) 300 and 3000 K. Temperature dependences (b) are calculated along the isobars (from top to bottom) 0 and 100 GPa. Solid line and dashed line — our calculations neglecting ELS (solid) and taking into account ELS (dashed). The inset at the top of right graph shows this dependence along the isobar 100 GPa.

and of the derivative of the specific surface energy with respect to the pressure: $\sigma'(P)_T = (\partial\sigma/\partial P)_T$. Figure 12 shows the dependences of the calculated function $\sigma'(P)_T$ (in 10^{-3} J/(m^{2}GPa)) on $B'(P)$. Figure 12, a shows these dependences calculated along the isotherms (from bottom to top) 300 and 3000 K. Figure 12, b shows these dependences calculated along the isobars 0 and 100 GPa. It can be seen that the dependences of the function $\sigma'(P)_T$ on the value $B'(P)$ are almost linear both along the isotherms and along the isobar $P = 0$ GPa. At the same time, taking into account ELS does not affect the pressure dependencies, but it leads to a decrease in this dependence along the isobar $P = 0$ GPa. This makes it possible to evaluate the magnitude $\sigma'(P)_T$ by the value $B'(P)$. However, along the isobars 100 GPa this dependence has a more complex form, as shown in the insert of Figure 12, a. Based on the presented results, it can be assumed that at a certain pressure $0 < P_B < 100$ GPa, the value of $B'(P)$ along the isobar P_B will not depend on $\sigma'(P)_T$.

5. Conclusion

A method has been developed for calculating the lattice and surface properties of a single-component crystal under any (corresponding to the solid phase) $P-T$ conditions. This method takes into account the contribution of both the lattice and electronic subsystems of the crystal. The method was tested by using analysis of BCC-Ta properties. Both the equation of state and $P-T$ dependences of the Debye temperature, the Grüneisen parameter, the isothermal elastic modulus the thermal expansion coefficient and the isobaric heat capacity were analyzed. Both the pressure dependences of these functions along the isotherms 300 and 3000 K and the temperature dependences along the isobars 0 and 100 GPa were obtained. It is shown that the analyzed dependences well agree with the data that are obtained both experimentally and by means of computer modelling.

This is the first study where the pressure and temperature dependences of the derivatives with respect to pressure of isothermal elastic modulus were calculated for BCC-Ta: $B'(P) = (\partial B_T/\partial P)_T$, thermal expansion coefficient: $\alpha'_p(P) = (\partial\alpha_p/\partial P)_T$, and isobaric heat capacity: $C'_p(P) = (\partial C_p/\partial P)T$. It was demonstrated that at certain pressure the isotherms $B'(P)$ are intersecting. It indicates that at this pressure the function $B'(P)$ does not depend on the temperature. It was shown that isobars $C'_p(P)$ have minimums and maximums.

It is shown that at a certain temperature (Birch temperature, T_B) the function $\alpha_p \cdot B_T$ does not change with isothermal pressure increase. At $T < T_B$, the function $\alpha_p \cdot B_T$ declines as the pressure goes up along the isotherm, and at $T > T_B$, the function $\alpha_p \cdot B_T$ rises with an isothermal increase in pressure. For BCC-Ta the Birch temperature makes 116.46 K, and doesn't depend on whether ELS has been taken int account or not.

For the first time the surface properties of BCC-tantalum at different $P-T$-conditions were found: the specific surface energy of the facet (100): $\sigma(100)$, its derivatives with respect to the temperature: $\sigma'(T)_i = (\partial\sigma/\partial T)_i$ (both the isochoric one: $i = v$, and the isobaric one: $i = P$) and the isothermal derivative of the function σ with respect to the pressure: $\sigma'(P)_T = (\partial\sigma/\partial P)_T$. Both the pressure dependences of these functions along the isotherms 300 and 3000 K and the temperature dependences along the

isobars 0 and 100 GPa were obtained. We have also obtained the estimates for the BCC-Ta fragmentation point at the various temperatures. It is shown that the function $\sigma'(P)_T$ for BCC-Ta linearly depends on the value of the isothermal derivative of the elastic modulus with respect to the pressure $B'(P)$.

It was demonstrated that when taking into account ELS the following properties are negligibly changed: $P(T, v)$, $\Theta(T, P)$, $\gamma(T, P)$, $q(T, P)$, $z(T, P) = = -(\partial \ln q/\partial \ln v)_T$, $B_T(T, P)$, $B'(P) = (\partial B_T/\partial P)_T$, Birch temperature, $\sigma(T, P)$, $\sigma'(T)_v = (\partial\sigma/\partial T)_v$, $\sigma'(P) = = (\partial\sigma/\partial P)_T$ and Δ_p. The function $\sigma'(P)$ versus $B'(P)$ shown in Figure 12 also is not changed. When taking ELS into account the following functions are noticeably varied: $\alpha_p(T, P) = (\partial \ln v/\partial T)_P$, $\alpha'_p(P) = (\partial\alpha_p/\partial P)_T$, $C_p(T, P)$, $C'_p(P) = (\partial C_p/\partial P)_T$, $\alpha_p \cdot B_T$, $\sigma'(T)_P = (\partial\sigma/\partial T)_P$. At the same time, as can be seen from Figure 4 and 6, when ELS is taken into account, the agreement of our calculated dependencies $\alpha_p(T, P)$ and $C_p(T, P)$ with experimental data improves markedly. However, as can be seen from Figures 4–7 and 10 with increase of the pressure along the isotherm 3000 K the contribution by the electron subsystem is reduced.

Acknowledgments

The author would like to thank S.P. Kramynin, K.N. Magomedov, Z.M. Surkhayeva and M.G. Yakhyaev for fruitful discussions and assistance in work.

Funding

This study was supported by the Russian Science Foundation, grant No. 25-23-00001, https://rscf.ru/project/25-23-00001/

Conflict of interest

The author declares that he has no conflict of interest.

References

[1] V.N. Senchenko, R.S. Belikov, V.S. Popov. J. Phys.: Conf. Ser. **653**, *1*, 012100 (2015). http://dx.doi.org/10.1088/1742-6596/653/1/012100
[2] H.K. Mao, J.A. Xu, P.M. Bell. J. Geophys. Res.: Solid Earth **91**, *B5*, 4673 (1986). http://dx.doi.org/10.1029/JB091iB05p04673
[3] K. Wang, R.R. Reeber. Mater. Sci. Eng.: R: Reports **23**, *3*, 101 (1998). http://dx.doi.org/10.1016/s0927-796x(98)00011-4
[4] H. Cynn, C.S. Yoo. Phys. Rev. B **59**, *13*, 8526.8529 (1999). http://dx.doi.org/10.1103/PhysRevB.59.8526
[5] A. Dewaele, P. Loubeyre, M. Mezouar. Phys. Rev. B **70**, *9*, 094112 (2004). http://dx.doi.org/10.1103/PhysRevB.70.094112
[6] P.I. Dorogokupets, A.R. Oganov. Phys. Rev. B **75**, *2*, 024115 (2007). http://dx.doi.org/10.1103/PhysRevB.75.024115
[7] Z.L. Liu, LC. Cai, X.R. Chen, Q. Wu, F.Q. Jing. J. Phys.: Condens. Matter **21**, *9*, 095408 (2009). http://dx.doi.org/10.1088/0953-8984/21/9/095408
[8] O.M. Krasil.nikov, Y.K. Vekilov, I.Y. Mosyagin. JETP **115**, *2*, 237 (2012). http://dx.doi.org/10.1134/S1063776112070096
[9] V.Y. Bodryakov. High Temperature **54**, *3*, 316 (2016). http://dx.doi.org/10.1134/S0018151X16030020
[10] J.W. Arblaster. J. Phase Equilibria. Diffusion **39**, *2*, 255 (2018). http://dx.doi.org/10.1007/s11669-018-0627-2
[11] H. Fukui, A. Yoneda, S. Kamada, H. Uchiyama, N. Hirao, A.Q.R. Baron. J. Appl. Phys. **132**, *5*, 055902 (2022). http://dx.doi.org/10.1063/5.0089667
[12] H. Liu, H. Song, H. Zhang, X. Duan, T. Zhang, H. Liu, Z. Wang, Y. Liu, S. Wang, Y. Li, L. Sun, W. Yang, Z. Guan, G. Zhang, D. Yang, J. Yang, Z. Zhao, H. Song, Y. Ding. J. Appl. Phys. **137**, *20*, 205905 (2025). https://doi.org/10.1063/5.0260857
[13] X. Gong, A. Dal Corso. J. Chem. Phys. **162**, *12*, 124709 (2025). https://doi.org/10.1063/5.0258989
[14] M.N. Magomedov. Phys. Solid State **63**, *10*, 1465(2021). https://doi.org/10.1134/S1063783421090250
[15] M.N. Magomedov. Phys. Solid State **64**, *7*, 765 (2022). https://doi.org/10.21883/PSS.2022.07.54579.319
[16] M.N. Magomedov. Phys. Rev. B **109**, *3*, 035405 (2024). http://dx.doi.org/10.1103/PhysRevB.109.035405
[17] E.A. Moelwyn-Hughes. Physical Chemistry. Pergamon Press, London (1961). 1333 p.
[18] C. Kittel. Introduction to Solid State Physics. J. Wiley & Sons Ltd, N.Y. (1976).
[19] V.N. Zharkov, V.A. Kalinin. Equations of State for Solids at High Pressures and Temperatures. Consultants Bureau-Plenum, N.Y. (1971).
[20] I.V. Lomonosov, S.V. Fortova. High Temperature **55**, *4*, 585 (2017). https://doi.org/10.1134/S0018151X17040113
[21] M.N. Magomedov. Tech. Phys. **58**, *9*, 1297 (2013). http://dx.doi.org/10.1134/S106378421309020X
[22] G.K. White, A.T. Pawlowicz. J. Low Temperature Phys. **2**, *5–6*, 631 (1970). https://doi.org/10.1007/BF00628279
[23] Y. Kraftmakher. Phys. Reports **299**, *2–3*, 79 (1998). https://doi.org/10.1016/S0370-1573(97)00082-3
[24] S. Mukherjee, R.E. Cohen, O G.lseren. J. Phys.: Condens. Matter **15**, *6*, 855 (2003). http://dx.doi.org/10.1088/0953-8984/15/6/312
[25] M.N. Magomedov. Tech. Phys. **68**, *2*, 209 (2023). https://doi.org/10.21883/TP.2023.02.55474.190-22
[26] M.N. Magomedov. Phys. Solid State **67**, *8*, 1389 (2025).
[27] H.A. Leupold, G.J. Iafrate, F. Rothwart, J.T. Breslin, D. Edmiston, T.R. AuCoin. J. Low Temperature Phys. **28**, *3*, 241 (1977). http://dx.doi.org/10.1007/BF00668217
[28] A. Dewaele. Minerals **9**, *11*, 684 (2019). http://dx.doi.org/10.3390/min9110684
[29] P.I. Dorogokupets, T.S. Sokolova, B.S. Danilov, K.D. Litasov. Geodynamics & Tectonophys. **3**, *2*, 129 (2012). (In Russian)
[30] M.G. Gorman, C.J. Wu, R.F. Smith, L.X. Benedict, C.J. Prisbrey, W. Schill, S.A. Bonev, Z.C. Long, P. Soderlind, D. Braun, D.C. Swift, R. Briggs, T.J. Volz, E.F. O.Bannon, P.M. Celliers, D.E. Fratanduono, J.H. Eggert, S.J. Ali, J.M. McNaney. Phys. Rev. B **107**, *1*, 014109 (2023). http://dx.doi.org/10.1103/PhysRevB.107.014109
[31] K. Wang, R.R. Reeber. High Temperature & Mater. Sci. **36**, *2–3*, 185 (1996).

[32] N.D. Milošević, G.S. Vuković, D.Z. Pavičić, K.D. Maglić. Int. J. Thermophys. **20**, 1129 (1999). http://dx.doi.org/10.1023/A:1022659005050
[33] A. Cezairliyan, J.L. McClure, C.W. Beckett. J. Res. National Bureau of Standards, Section A, Phys. Chem. **75A**, *1*, 1 (1971). http://dx.doi.org/10.6028/jres.075A.001
[34] F. Birch. J. Geophys. Res. **57**, *2*, 227 (1952). http://dx.doi.org/10.1029/JZ057i002p00227
[35] O.L. Anderson. Phys. Earth & Planetary Interiors **22**, *3–4*, 165 (1980). http://dx.doi.org/10.1016/0031-9201(80)90029-1
[36] J. Rault. Eur. Phys. J. B **92**, *1*, 22 (2019). http://dx.doi.org/10.1140/epjb/e2018-90452-6
[37] W.R. Tyson. Canadian Metallurgical Quarterly **14**, *4*, 307 (1975). https://doi.org/10.1179/000844375795049997
[38] W.R. Tyson, W.A. Miller. Surf. Sci. **62**, 267 (1977). https://doi.org/10.1016/0039-6028(77)90442-3
[39] L.Z. Mezey, J. Giber. Japan. J. Appl. Phys. **21**, *11R*, 1569 (1982). http://dx.doi.org/10.1143/jjap.21.1569
[40] V.K. Kumikov, Kh.B. Khokonov. J. Appl. Phys. **54**, *3*, 1346 (1983). https://doi.org/10.1063/1.332209
[41] M.I. Baskes. Phys. Rev. B **46**, *5*, 2727 (1992). https://doi.org/10.1103/PhysRevB.46.2727
[42] L. Vitos, A.V. Ruban, H.L. Skriver, J. Koll.r. Surf. Sci. **411**, *1–2*, 186 (1998). https://doi.org/10.1016/S0039-6028(98)00363-X
[43] A.B. Alchagirov, B.B. Alchagirov, T.M. Taova, Kh.B. Khokonov. Trans. JWRI **30**, *Special Issue*, 287 (2001). https://repository.exst.jaxa.jp/dspace/handle/a-is/48071
[44] Q. Jiang, H.M. Lu, M. Zhao. J. Phys.: Condens. Matter **16**, *4*, 521 (2004). https://doi.org/10.1088/0953-8984/16/4/001
[45] F. Aqra, A. Ayyad. Appl. Surf. Sci. **257**, *15*, 6372 (2011). https://doi.org/10.1016/j.apsusc.2011.01.123
[46] V.P. Bokarev, G.Y. Krasnikov. Surf. Sci. **668**, 73 (2018). https://doi.org/10.1016/j.susc.2017.10.020
[47] J.-Y. Lee, M.P.J. Punkkinen, S. Schönecker, Z. Nabi, K. Kádas, V. Zólyomi, Y.M. Koo, Q.-M. Hu, R. Ahuja, B. Johansson, J. Koll.r, L. Vitos, S.K. Kwon. Surf. Sci. **674**, 51 (2018). https://doi.org/10.1016/j.susc.2018.03.008
[48] C. Li, S. Lu, S. Divinski, L. Vitos. Acta Materialia **255**, 119074 (2023). https://doi.org/10.1016/j.actamat.2023.119074
[49] S.N. Zhevnenko, I.S. Petrov, D. Scheiber, V.I. Razumovskiy. Acta Materialia **205**, 116565 (2021). https://doi.org/10.1016/j.actamat.2020.116565
[50] M.N. Magomedov. Phys. Solid State **67**, *2*, 333 (2025). https://doi.org/10.61011/PSS.2025.02.60685.318

Translated by T.Zorina